Atmos. Chem. Phys. Discuss., 10, 15167–15196, 2010
www.atmos-chem-phys-discuss.net/10/15167/2010/
doi:10.5194/acpd-10-15167-2010

Atmospheric Chemistry and Physics Discussions

Aircraft observations of enhancement and depletion of black carbon mass in the springtime Arctic

J. R. Spackman[1,2], R. S. Gao[1], W. D. Neff[3], J. P. Schwarz[1,2], L. A. Watts[1,2], D. W. Fahey[1,2], J. S. Holloway[1,2], T. B. Ryerson[1], J. Peischl[1,2], and C. A. Brock[1]

[1]National Oceanic and Atmospheric Administration, Earth System Research Laboratory, Chemical Sciences Division, Boulder, Colorado, USA
[2]Cooperative Institute for Research in Environmental Sciences, University of Colorado, Boulder, Colorado, USA
[3]National Oceanic and Atmospheric Administration, Earth System Research Laboratory, Physical Sciences Division, Boulder, Colorado, USA

Received: 29 May 2010 – Accepted: 1 June 2010 – Published: 21 June 2010

Correspondence to: J. R. Spackman (ryan.spackman@noaa.gov)

Published by Copernicus Publications on behalf of the European Geosciences Union.

Abstract

Understanding the processes controlling black carbon (BC) in the Arctic is crucial for evaluating the impact of anthropogenic and natural sources of BC on Arctic climate. Vertical profiles of BC mass were observed from the surface to near 7-km altitude in April 2008 using a Single-Particle Soot Photometer (SP2) during flights on the NOAA WP-3D research aircraft from Fairbanks, Alaska. These measurements were conducted during the NOAA-sponsored Aerosol, Radiation, and Cloud Processes affecting Arctic Climate (ARCPAC) project as part of POLARCAT, an International Polar Year (IPY) activity. In the free troposphere, the Arctic air mass was influenced by long-range transport from biomass-burning and anthropogenic source regions at lower latitudes especially during the latter part of the campaign. Maximum average BC mass loadings of 150 ng kg^{-1} were observed near 5.5-km altitude in the aged Arctic air mass. In biomass-burning plumes, BC was enhanced from near the top of the Arctic boundary layer (ABL) to 5.5 km compared to the aged Arctic air mass. At the bottom of some of the profiles, positive vertical gradients in BC were observed in the vicinity of open leads in the sea-ice. BC mass loadings increased by about a factor of two across the boundary layer transition in the ABL in these cases while carbon monoxide (CO) remained constant, evidence for depletion of BC in the ABL. BC mass loadings were positively correlated with O_3 in ozone depletion events (ODEs) for all the observations in the ABL suggesting that BC was removed by dry deposition of BC on the snow or ice because molecular bromine, Br_2, which photolyzes and catalytically destroys O_3, is thought to be released near the open leads in regions of ice formation. We estimate the deposition flux of BC mass to the snow using a box model constrained by the vertical profiles of BC in the ABL. The open leads may increase vertical mixing in the ABL and entrainment of pollution from the free troposphere possibly enhancing the deposition of BC to the snow.

ACPD

10, 15167–15196, 2010

1 Introduction

Black carbon (BC) in the Arctic directly contributes to regional climate change through radiative heating of the atmosphere and warming at the snow surface due to absorption of incoming solar shortwave radiation (Shindell and Faluvegi, 2009; McConnell et al., 2007; Hansen and Nazarenko, 2004). Despite the dimming caused by the absorption of solar radiation by BC aerosol aloft, BC deposited in snow has been shown to exacerbate Arctic warming through the snow albedo effect, a process whereby surface warming causes snow and ice removal leading to a decrease in the surface albedo that triggers additional warming (Flanner et al., 2007, 2009). The fourth assessment of the Intergovernmental Panel on Climate Change reported that BC in snow accounts for a forcing of 0.1 $W\,m^{-2}$ with a factor of two in uncertainty (IPCC, 2007). Measurements of BC in the Arctic troposphere above the surface are both limited and needed to constrain transport and microphysics in global aerosol models to better evaluate climate impacts (Koch et al., 2009; Shindell et al., 2008).

Enhancements of BC and other tracers of pollution have been observed for decades in the Arctic troposphere in the winter and early spring (Hansen and Novakov, 1989; Sharma et al., 2006; Law and Stohl, 2007; Koch et al., 2009). These enhancements emerge from the chemistry and dynamics unique to this region. Aerosols and tracers are generally longer lived in the Arctic in winter and early spring than at other times because of colder temperatures and weaker solar insolation. Secondly, the high latitudes are isolated from lower latitudes in winter by the polar jet that induces a weak meridional barrier to transport in the troposphere (Stohl, 2006). Together, these phenomena lead to an increase in BC aerosol in the Arctic air mass we refer to as aged Arctic air in this work.

BC aerosol is produced from incomplete fossil-fuel and biomass-burning combustion processes and is largely emitted at lower latitudes and then transported into the Arctic along isentropic surfaces (Stohl, 2006). Some modeling studies suggest anthropogenic sources from Europe and Asia maintain the enhanced level of pollution at northern

ACPD
10, 15167–15196, 2010

high latitudes often referred to as Arctic haze (Quinn et al., 2007; Koch and Hansen, 2005). A number of other works have shown how transport of biomass-burning plumes from agricultural and forest fires at midlatitudes contribute to Arctic haze particularly in spring (Warneke et al., 2009; Generoso et al., 2007; Kaneyasu et al., 2007). The blend of anthropogenic and biomass burning influenced air masses in the springtime Arctic largely depends on interannual variability in biomass burning at northern midlatitudes (Warneke et al., 2010).

The seasonally enhanced BC loadings in the Arctic free troposphere may lead to increased wet and dry deposition of BC to the snow or ice through scavenging followed by precipitation and removal by direct contact with the snow or ice surface, respectively. While BC is observed in snow at sites throughout northern high latitudes (e.g., Hegg et al., 2009), scattering aerosol such as sulfate may be preferentially scavenged leaving behind BC aerosol suspended in the atmosphere. In this case, dry deposition may play an important role in depositing BC to the snow. Atmospheric perturbations that facilitate the mixing of BC from the free troposphere into the Arctic boundary layer (ABL), such as through open leads or enhanced vertical wind shear, might then lead to increased deposition of BC to the snow.

Here we present vertical profiles of BC mass in the troposphere in the springtime Arctic using data from a Single-Particle Soot Photometer (SP2) to measure the refractory mass of individual BC particles. We first show enhancements of BC mass in the free troposphere in biomass-burning plumes relative to the aged Arctic air mass and then focus on the observed depletions of BC mass in the ABL over the snow and ice north of Alaska in the rest of the paper. We present the correlations between simultaneous measurements of BC mass, carbon monoxide (CO) and ozone (O_3) in the ABL to examine the processes controlling the removal of BC. Lastly, we use a simple box model constrained by the observed vertical profiles of BC to bound the flux of BC from the free troposphere to the snow or ice surface.

ACPD
10, 15167–15196, 2010

2 Aircraft measurements

The NOAA WP-3D research aircraft deployed to Fairbanks, Alaska (65° N, 148° W) in April 2008 for the Aerosol, Radiation, and Cloud Processes affecting Arctic Climate (ARCPAC) campaign (Brock et al., 2010). ARCPAC occurred during POLARCAT as part of the International Polar Year (IPY) research activities in the Arctic. POLARCAT is the Polar Study using Aircraft, Remote Sensing, Surface Measurement and Models, of Climate, Chemistry, Aerosols, and Transport. We present measurements of BC mass loadings, CO, O_3, and meteorological parameters from 5 flights in the Arctic, 12–21 April 2008, spanning 0–7.4 km in altitude, 65–75° N in latitude, and 126–165° W in longitude (Fig. 1). The aircraft probed the ABL, usually less than 300 m in depth, mostly over the ice and open leads north of Alaska for ~7 h in the data used here.

The SP2 measures the refractory BC mass in individual BC-containing particles using laser-induced incandescence, whereby the BC-fraction is heated to its boiling point and the thermal radiation, or incandescence, emitted by the intensely hot material is detected (Schwarz et al., 2006). The measurement of refractory mass is continuous, BC-specific, proportional to the incandescence signal, and independent of particle mixing state and morphology (Slowik et al., 2007). BC mass loading is reported as a mass mixing ratio in ng-(kg dry air)$^{-1}$. For the data presented here, the SP2 detected BC particles in the size range of 90- to 600-nm volume-equivalent diameter (VED), based on a void-free density of 2 g cm^{-3} for ambient BC aerosol. This range includes ~90% of the BC mass and ~50% of the number of BC particles assuming a log-normal distribution of BC mass in the fine mode peaked near 200 nm (Schwarz et al., 2006). The measured BC mass mixing ratios reported in this work have been multiplied by 1.1 to account for the unmeasured mass outside the SP2 detection range. The SP2 sampled ambient aerosol behind a 1-μm particle impactor through a low-turbulence inlet. Data from the PALMS instrument, a single-particle laser mass spectrometer, indicating cloud contamination of its aerosol inlet (Froyd et al., 2010) were used to remove the SP2 data acquired during these sampling times. The uncertainty of the reported BC

ACPD
10, 15167–15196, 2010

mass loadings during ARCPAC is approximately 40% attributed primarily to uncertainty in BC mass calibration with a lesser contribution from sample flow uncertainty.

In situ measurements of CO were acquired at 1 Hz by a vacuum ultraviolet resonance fluorescence instrument with an uncertainty of ±5% (Holloway et al., 2000). O_3 was measured with a NO-induced chemiluminescence technique with an estimated uncertainty of ±(0.05 ppb+4%) for the 1-Hz data (Ryerson et al., 1998).

3 Observations of BC mass loadings in the Arctic troposphere

Airborne BC measurements in the Arctic troposphere were limited prior to the POLARCAT campaigns in 2008 and consisted mostly of filter-based absorption techniques sampling bulk aerosol (Hansen and Rosen, 1984; Hansen and Novakov, 1989). In addition to the measurements presented in this work, two other SP2 instruments aboard the NASA DC-8 and P3-B research aircraft collected single-particle BC data in spring 2008 during the NASA-sponsored Arctic Research of the Composition of the Troposphere from Aircraft and Satellites (ARCTAS) campaign (Jacob et al., 2010). The NOAA WP-3D probed the ABL around open leads north of Alaska for longer time than either NASA aircraft which sampled a larger geographical area of the Arctic.

3.1 Enhancement of BC mass in the free troposphere

The observed vertical profiles of BC mass from 5 flights in the Arctic are shown in Fig. 2. The individual data points are 30-s averages of BC mass each representing a horizontal spatial resolution of ~3 km. The data in blue were collected on the 12 April 2008 flight in the aged Arctic air mass and the data in red were acquired on 4 flights (15–21 April) in air strongly influenced by long-range biomass burning plumes. The free tropospheric region sampled by the NOAA WP-3D aircraft was frequently influenced by long-range biomass burning plumes from Kazakhstan and Siberia during ARCPAC (Warneke et al., 2009). The mean BC mass loadings, noted by the lines with whiskers,

ACPD
10, 15167–15196, 2010

increase with altitude in the springtime Arctic with BC enhancements of a factor of 2 to 4 with increasing altitude from the lower to upper troposphere. This important observation constrains global aerosol models that generally underestimate the advection of BC to the Arctic (Koch et al., 2009). The BC mass loadings in the middle troposphere are comparable to those observed in the planetary boundary layer in a polluted urban environment in the United States. Although one would not necessarily expect agreement because of natural variability in long-range transport and changes in emissions over time, the profiles obtained with the SP2 generally show lower BC mass loadings compared to those from an aethalometer during the Arctic Gas and Aerosol Sampling Programs (AGASP) campaigns conducted in 1983 and 1986 (see black trace in Fig. 7f in Stone et al., 2010 based on results from Hansen and Novakov, 1989). The ARCPAC profiles show distinct enhancements in BC mass in the middle and upper troposphere compared to the lower troposphere unlike the AGASP-I composite profile that indicates a polluted lower troposphere and decreasing BC loadings with increasing altitude.

These Arctic profiles contrast with profiles at midlatitudes (Spackman et al., 2008) and in the tropics (not shown) (Schwarz et al., 2008) where BC mass generally decreases by 2–3 orders of magnitude from the surface to 5-km altitude, given by the black line in Fig. 2. These profiles may still be consistent because the tropics and midlatitudes are linked to high latitudes by meridional exchange along isentropic surfaces (Stohl, 2006; Quinn et al., 2007). Since an air parcel is lofted in altitude as it is advected poleward, pollution in the lower troposphere at midlatitudes maps to the middle troposphere at high latitudes in the absence of diabatic processes during transport.

3.2 Depletion of BC mass in the ABL

Vertical profiles of BC mass and CO are shown in detail in Fig. 3 for the lowest 2 km of the flight tracks displayed in Fig. 1. Each flight includes one ascent profile from and one descent profile into Fairbanks with local pollution influence, marked by the red points, with the normally observed decrease in BC mass with increasing altitude above a polluted boundary layer. The profiles denoted by the blue points are mostly north of

ACPD
10, 15167–15196, 2010

Alaska over the ice and open leads. A large positive but variable vertical gradient in BC mass was observed in the lowest few hundred meters over the ice and open leads on several of the flights. The mean profiles with one standard deviation are shown by the black lines with bars. BC mass increases by up to a factor of 5 from the minimum observed altitude in the ABL up to 700 m in the free troposphere, observed on 12, 18, 21 April. Figure 3 is a composite of all the vertical gradients in BC and CO and offers some indication of the persistence of the BC gradient during multiple profiles. These data include both spiral and slantwise flight profiles; the latter profiles may add horizontal variability to the results. While the WP-3D aircraft extensively sampled the ABL, there are limited profile data between this layer and the free troposphere with widely varying aerosol and chemical compositions during the sampling periods especially on 18–21 April.

Since BC and CO are both byproducts of incomplete combustion, they are often well correlated in the troposphere (e.g., Spackman et al., 2008). As shown in Fig. 3, on the 12 April flight in the aged Arctic air mass, Northern Hemisphere springtime high-latitude background values of CO (~160 ppb) persisted throughout most of the lowest 2 km while BC mass increased by a factor of 2 to 3 from 100- to 500-m altitude. The observed gradient in BC with respect to constant values of CO indicates that the lower BC mass loadings in the ABL cannot be explained by air mass advection in which a cleaner air mass with less BC and CO is mixed into the ABL from the free troposphere. Rather, the simultaneous measurements are consistent with the physical removal of BC aerosol from this air mass through deposition. The processes controlling BC in the ABL will be explored in greater detail using BC–CO and O_3–BC correlations in Sect. 4. Note that two other aerosol instruments (for details of the NMASS and UHSAS instruments, see Brock et al., 2004) aboard the WP-3D aircraft that measure particle number and size distributions showed evidence for particle removal in the ultrafine and fine modes (i.e., 4–1000 nm).

Polluted midlatitude air began to influence the sampling region on the 15 April flight, effectively pushing the aged Arctic air further north for most of the remainder of the

ACPD
10, 15167–15196, 2010

campaign. An analysis using chemical signatures and FLEXPART, a Lagrangian particle dispersion model, attributes most of the pollution in the midlatitude air to agricultural and forest fires in Kazakhstan and the Lake Baikal region of Siberia, respectively (Warneke et al., 2009). Most of these plumes were observed above 2-km altitude but some can be seen in Fig. 3, characterized by higher values of BC mass and enhanced CO above background, especially on 19 April. Note the free troposphere is largely decoupled from the ABL on the timescales of several days during which these measurements were taken. Less than 1% of the data points sampled in the ABL (<300 m altitude) during ARCPAC are characterized by CO values greater than 200 ppb, the criterion used here to denote sampling of anthropogenic or biomass-burning plumes. These few data were mostly collected on ascent from and descent into Fairbanks and from the 19 April flight over the sea-ice immediately north of Barrow. Ozonesonde data from the NOAA Global Monitoring Division (GMD) baseline site at Barrow on this date indicated biomass-burning plumes mixed down to the surface (S. Oltmans, private communication) consistent with the BC and CO data in Fig. 3. This event removed all evidence of BC vertical gradient in the ABL on this date.

A BC vertical gradient approaching a factor of 5 was observed on 18 and 21 April. Given the prevalence of biomass-burning plumes streaming through the free troposphere and the decoupled ABL during this period, the observed gradients from these flights cannot be completely attributed to depletion. The enhanced CO values of 180 to 220 ppb at the top of the BC vertical gradient on these flights support this conclusion. To avoid the complication from the advection of polluted air masses, the depositional loss is quantified based on boundary layer flight segments on 12 April in the aged Arctic air mass. The time series of altitude, latitude, O_3, CO, BC mass, and sea-surface temperature (SST) for the 12 April flight are shown in Fig. 4. SST is a remote sensing measurement of the temperature at the sea-ice or open water surface when the aircraft is a couple kilometers or less above the surface. The spikes in the SST data in the shaded regions of Fig. 4 indicate the aircraft is flying repeatedly over the sea-ice and open leads. We include O_3 data here because O_3 is typically depleted in the ABL

ACPD
10, 15167–15196, 2010

over the snow and ice due to bromine-catalyzed O_3 destruction (Simpson et al., 2007) coincident with the observations of BC removal. Note the nearly complete removal of O_3 in the second and third segments. This correlation will be discussed in more detail in the next section in the context of the BC mass depletions.

Low-altitude profile segments for the shaded regions in Fig. 4 are shown in Fig. 5 for BC, CO, O_3, and potential temperature. The red-shaded region in Fig. 5 marks the ABL and is chosen based on where the ascent and descent profiles of potential temperature converge. In both Fig. 5b and c, there is a positive vertical gradient in BC mass loading in the ABL which is well correlated with ozone depletion and generally occurs in the vicinity of open leads in the sea-ice. As mentioned earlier, this gradient occurs while CO is unvarying. In Fig. 5b, the spiral ascent (red) and slantwise descent data (blue) are shown separately because of the variability in the free troposphere over the geographical area of the profiles. In Fig. 5a, note the limited BC data in the ABL prevent any conclusions from these particular profiles. We use the average ascent profile in Fig. 5b to estimate BC removal at $\sim$15 ng kg^{-1} based on the difference between the average BC mass mixing ratios at the top and bottom of the profile. This is roughly consistent with the observed gradient shown in Fig. 5c despite the larger variability in BC over the depth of the ABL. We use this observed quantity to calculate a deposition flux of BC to the snow in Sect. 4.

4 BC deposition

The processes controlling BC aerosol in the ABL include long-range transport and deposition. Since there are limited anthropogenic sources and it is too early for biomass burning in the springtime Arctic, most of the BC reaches the ABL from lower latitudes by advection in the free troposphere followed by slow mixing into the ABL. Loss processes for BC aerosol include wet and dry deposition. Wet deposition might occur in the saturated layer at the top of the ABL or in cloud layers in the free troposphere while dry deposition occurs by BC particles coming in direct contact with snow or ice through mixing processes in the ABL.

ACPD
10, 15167–15196, 2010

Sampling over open leads or in lead-influenced air may play a role in BC removal. Open leads perturb the stable ABL because the temperature difference between the ice and the liquid water induces convection over and downstream of the lead (Anderson and Neff, 2008). Open leads may enhance (i) mixing in the ABL facilitating the deposition of BC to the snow or ice and (ii) entrainment of air from the free troposphere which is often polluted in the springtime Arctic due to long-range transport. However, the ARCPAC dataset essentially shows no evidence for (ii), at least for the limited time the NOAA WP-3D was sampling in the vicinity of the open leads (Brock et al., 2010).

Although open leads also inject water vapor into the ABL, clouds were generally not observed over the open leads during ARCPAC because many of the leads were observed to be at least partially covered with thin ice (Brock et al., 2010). The leads were still a major moisture source to the ABL and diamond dust may have played a role in the removal of BC through dry deposition on these ice crystals or through a wet removal process whereby BC particles act as ice nuclei. However, the latter mechanism was not observed for total aerosol in the ultrafine and fine modes during ARCPAC (Brock et al., 2010). Because it was difficult to unambiguously identify open-lead influenced air in the aircraft data, we cannot definitively comment on the potential role of open leads in the removal of BC with this dataset.

4.1 Observational evidence for BC deposition

As shown in Fig. 6, BC and CO values are generally well correlated in the free troposphere for the 21 April flight. The 30-s data have been segregated by altitude to highlight the data below 750-m altitude in red. These lower altitude data, from the region of the large BC vertical gradient, fall off the BC–CO line consistent with a process of BC removal in the ABL. This feature in the correlation was also observed for the data on 12 and 18 April but we only show the data from 21 April because of the larger dynamic range in CO on this flight.

ACPD
10, 15167–15196, 2010

The O_3–BC correlation for all the flights is shown in Fig. 7. The 30-s data are color-coded by altitude. Ozone is positively correlated with BC for the main body of points (i.e., O_3>40 ppb, BC>30 ng kg^{-1}), associated with biomass-burning plumes and anthropogenic pollution. Two additional positive correlations exist in this figure in (i) the ABL in ozone depletion events (ODEs) and (ii) a shallow mixing layer at the top of the ABL. In the ODEs, O_3 is removed through catalytic destruction by bromine (Simpson et al., 2007). In (i), the black points for 0<O_3<40 ppb and 15<BC<30 ng kg^{-1}, more processed air contains less BC. In the ODEs, in general lesser amounts of O_3 in Fig. 7 relate to lower altitude in the ABL and greater amounts of O_3 are nearer the top of the ABL. In (ii), the black points embedded in the main body of data points for 40<O_3<55 ppb and 30<BC<200 ng kg^{-1}, the correlation is a mixing line between the air masses in the ABL and the free troposphere. Note the O_3–BC correlation in ODEs is robust over the course of 5 flights spanning 10 days with a total of 7 h sampling in the ABL. Enhancements of Br_2, representative of active bromine, were observed in the ODEs during ARCPAC (Neuman et al., 2010). The general theory is that Br_2 is released to the atmosphere from the brine during sea-ice formation so the correlation between O_3 and BC mass suggests BC particles have been preferentially removed by contact with the snow. The competing hypothesis that wet scavenging removes BC in the vicinity of open leads is less likely because the positive correlation between O_3 and BC would not be expected if ice crystals were scavenging BC particles through the depth of the ABL or even preferentially at the top of the ABL.

Dry deposition might be expected to preferentially remove large BC particles in the ABL. However, the size distributions (not shown) of BC mass for both the ABL and free troposphere flight segments shown in Fig. 4 are essentially the same. The mode for both these mass distributions is ~160 nm, significantly smaller than the ~200 nm mode observed on 18 April in the free troposphere when biomass-burning plumes were present. The similarity between size distributions on 12 April does not necessarily contradict the premise of BC removal by dry deposition because the statistical sampling is probably inadequate to draw any conclusion. On the other hand, the size distributions

ACPD
10, 15167–15196, 2010

support the CO data that indicate similar sources across the boundary layer transition.

4.2 BC deposition flux

We now place the observations in the context of what is expected from mixing processes in the springtime ABL. The first two profiles in the schematic in Fig. 8 are idealized cases assuming BC is predominantly removed by dry deposition. In the first case, rapid ABL mixing delivers BC to the snow surface where removal occurs faster than BC can be imported from the free troposphere. This results in a step-wise decrease in BC mass below the top of the ABL. In the second case, BC is mixed from the free troposphere into the ABL as fast or faster than ABL mixing delivers BC to the surface leading to a constant value of BC through most of the ABL. In this case, removal of BC occurs in a shallow layer at the surface where the BC-containing air mass is in direct contact with the surface. The third profile in the schematic qualitatively represents what was observed on multiple profiles in the ABL on 12, 18, and 21 April. The largest BC gradient is generally observed at the top of the ABL corresponding to the mixing line between O_3 and BC in the tracer-tracer correlation in Fig. 7. The BC gradient in the observed profile in Fig. 8 extends over a range of 250 to 750 m depending on the specific profile. Although the measurements do not cleanly fit into either idealized case, they are clearly more consistent with the profiles depicted by the fast ABL mixing case.

We now use a simple box model to estimate the deposition flux of BC to the snow. A coupled system of linear differential equations is formulated to describe the flux of BC from the free troposphere into the ABL and removal by contact with the surface. Figure 9 shows a schematic of this 4-box system. The aged Arctic air mass in the free troposphere is represented by the BC mass loading in C_4. The ABL is represented by the BC mass loadings, C_3–C_1, in 3 boxes. The free-troposphere-to-boundary-layer exchange coefficient, k_{FT}, is proportional to the flux of BC mass from the free troposphere to the ABL, and the ABL exchange coefficient, k_{BL}, scales with the downward flux of BC mass through the ABL and to the snow. Since the observations indicate the timescale for mixing between the free troposphere and ABL is longer than the ABL

ACPD
10, 15167–15196, 2010

turnover timescale, k_{BL} is larger than k_{FT}. One other variable in this problem is the removal efficiency of BC when it contacts the snow. This removal efficiency factor is used in the model to scale the flux of BC mass, C_1, to the snow.

If we assume a range of values for k_{BL} corresponding to e-folding timescales of 1 to 8 h, we can solve the system of differential equations uniquely for k_{FT} and the removal efficiency as shown in Fig. 10 for the 12 April flight. The model better reproduces the BC vertical profiles in the ABL for removal efficiency factors between 0.01 and 0.1. These values confine most, but not all, of the BC gradient to the boundary layer transition consistent with the O_3-BC correlation. With 5% removal efficiency, the e-folding timescales for exchange between the free troposphere and boundary layer are computed to be a 10 times longer than the assumed e-folding timescale for the boundary layer turnover. A tracer-tracer correlation of O_3 and CO (not shown) indicates the biomass-burning plumes streaming through the free troposphere 15–21 April generally did not mix into the ABL, except the synoptic-scale event on 19 April mentioned earlier, which points toward even longer free-troposphere-to-boundary-layer timescales than suggested by the simple box model results. For instance, a plausible ABL turnover time of 2 h implies a 20-h timescale for free-troposphere-to-boundary-layer exchange. A possible reason for this discrepancy may be that the physical mixing processes are less likely continuous as modeled and more likely episodic as the temperature difference between the sea-ice and open leads interact with meteorology. During the ARCPAC sampling period, the WP-3D may not have sampled these episodic exchange processes.

Since mixing of BC from the free troposphere into the ABL is the rate-limiting step to deposit BC to the surface, we can use a range of model-derived timescales (i.e., k_{FT}) to calculate deposition fluxes for BC to the snow. Based on the profile segments shown in Fig. 5b, BC removal is $\sim$15 ng kg^{-1} over the depth of the ABL, about 300 m. For a range of possible boundary layer turnover times, 1 to 8 h, the corresponding free-troposphere-to-boundary-layer exchange is 10 to 80 h. The corresponding deposition fluxes are 170 to 1700 ng (m^2 day)$^{-1}$. We can relate these calculated deposition fluxes to measured

ACPD
10, 15167–15196, 2010

BC mass loading in snow. When deposition occurs, we assume the snow exposed to the air is still fresh and uncompacted with a density of 100 kg m^{-3} when deposition occurs. This is probably reasonable based on the climate data (1971–2000) at Barrow, representative of weather conditions over the Arctic ocean north of the site where the aircraft measurements were taken. The meteorological surface data at Barrow indicate an average 5.3-cm snow accumulation with measureable snow an average of 18 days in April. Based on the dry deposition fluxes calculated here, this equates to between 1 and 10 ng-BC (g-snow)$^{-1}$. These derived values are plausible with respect to the recent published results of ~2 to 10 ng g^{-1} in the Alaskan Arctic (Hegg et al., 2009). A contribution of BC to the snow from precipitation scavenging would increase the values derived here but these are still likely consistent with the large range of literature values for BC in snow across the Arctic (Flanner et al., 2007). The large variability in the reported BC loadings in snow may be partly explained by the interannual and seasonal variability in the amount of snowfall at a given site.

5 Summary

Single-particle measurements of BC mass mixing ratios from the NOAA WP-3D research aircraft were acquired from the ground to about 7 km in the springtime Arctic showing an increase of BC mass with increasing altitude from the ABL to the middle and upper troposphere. These BC aerosol measurements in the Arctic provide important constraints on global aerosol models (Koch et al., 2009). In the lowest 700 m over the sea ice, a positive vertical gradient in BC mass was observed in many of the profiles suggesting removal of BC through deposition to the snow surface. BC mass and CO are well correlated throughout the free troposphere except in the ABL when BC depletions were observed. Ozone and BC are positively correlated in ozone depletion events suggesting that BC mass is removed through dry deposition. Using a box model constrained by the BC measurements from a flight prior to the advection of biomass burning plumes to the Arctic, we estimate a deposition flux of BC between 170 and

ACPD
10, 15167–15196, 2010

1700 ng $(m^2\,day)^{-1}$ corresponding to boundary layer e-folding turnover timescales of 1 to 8 h, respectively. Based on long-term average meteorology at Barrow in April, this result is consistent with the results from Hegg et al. (2009). Enhanced deposition may be occurring in regions influenced by open leads in the ice because the open leads facilitate mixing between the free troposphere and ABL, the rate-limiting step for delivering BC aerosol to the surface of the snow. These observations are important to understanding the processes controlling BC in the ABL that have important implications for Arctic climate.

Acknowledgements. We are grateful to K. Froyd and S. Lance for PALMS and cloud probe data, respectively, used to exclude cloud sampling from the black carbon data. We also thank J. Cozic for particle number concentration data supporting this analysis. This research was supported by the NOAA Atmospheric Composition and Climate Program and the NASA Radiation Sciences Program.

References

Anderson, P. S. and Neff, W. D.: Boundary layer physics over snow and ice, Atmos. Chem. Phys., 8, 3563–3582, doi:10.5194/acp-8-3563-2008, 2008.

Brock, C. A., Hudson, P. K., Lovejoy, E. R., Sullivan, A., Nowak, J. B., Huey, L. G., Cooper, O. R., Cziczo, D. J., de Gouw, J., Fehsenfeld, F. C., Holloway, J. S., Hubler, G., Lafleur, B. G., Murphy, D. M., Neuman, J. A., Nicks, D. K., Orsini, D. A., Parrish, D. D., Ryerson, T. B., Tanner, D. J., Warneke, C., Weber, R. J., and Wilson, J. C.: Particle characteristics following cloud-modified transport from Asia to North America, J. Geophys. Res., 109, D23S26, doi:10.1029/2003JD004198, 2004.

Brock, C. A., Cozic, J., Bahreini, R., Brioude, J., de Gouw, J. A., Fahey, D. W., Ferrare, R., Froyd, K. D., Holloway, J. S., Hubler, G., Lack, D., Lance, S., Middlebrook, A. M., Montzka, S. A., Murphy, D. M., Neuman, J. A., Nowak, J., Peischl, J., Pierce, B., Ryerson, T. B., Schwarz, J. P., Sodemann, H., Spackman, J. R., Stocks, B., Stohl, A., Veres, P., and Warneke, C.: Characteristics, sources, and transport of aerosols measured in spring 2008 during the Aerosol, Radiation, and Cloud Processes Affecting Arctic Climate (ARCPAC) project, Atmos. Chem. Phys. Discuss., in preparation, 2010.

ACPD

10, 15167–15196, 2010

Flanner, M. G., Zender, C. S., Randerson, J. T., and Rasch, P. J.: Present-day climate forcing and response from black carbon in snow, J. Geophys. Res., 112, D11202, doi:10.1029/2006JD008003, 2007.

Flanner, M. G., Zender, C. S., Hess, P. G., Mahowald, N. M., Painter, T. H., Ramanathan, V., and Rasch, P. J.: Springtime warming and reduced snow cover from carbonaceous particles, Atmos. Chem. Phys., 9, 2481–2497, doi:10.5194/acp-9-2481-2009, 2009.

Froyd, K. D., Murphy, D. M., Lawson, P., Baumgardner, D., and Herman, R. L.: Aerosols that form subvisible cirrus at the tropical tropopause, Atmos. Chem. Phys., 10, 209–218, doi:10.5194/acp-10-209-2010, 2010.

Generoso, S., Bey, I., Attié, J.-L., and Bréon, F.-M.: A satellite- and model-based assessment of the 2003 Russian fires: Impact on the Arctic region, J. Geophys. Res., 112, D15302, doi:10.1029/2006JD008344, 2007.

Hansen, A. D. A. and Novakov, T.: Aerosol black carbon measurements in the Arctic haze during AGASP-II, J. Atmos. Chem., 9, 347–361, 1989.

Hansen, A. D. A. and Rosen, H.: Vertical distributions of particulate carbon, sulfur, and bromine in the Arctic haze and comparison with ground-level measurements at Barrow, Alaska, Geophys. Res. Lett., 11(5), 381–384, 1984.

Hansen, J. and Nazarenko, L.: Soot climate forcing via snow and ice albedos, P. Natl. Acad. Sci. USA, 101, 423–428, 2004.

Hegg, D. A., Warren, S. G., Grenfell, T. C., Doherty, S. J., Larson, T. V., and Clarke, A. D.: Source attribution of black carbon in Arctic snow, Environ. Sci. Technol., 43(11), 4016–4021, doi:10.1021/es803623f, 2009.

Holloway, J. S., Jakoubek, R. O., Parrish, D. D., Gerbig, C., Volz-Thomas, A., Schmitgen, S., Fried, A., Wert, B., Henry, B., and Drummond, J. R.: Airborne intercomparison of vacuum ultraviolet fluorescence and tunable diode laser absorption measurements of tropospheric carbon monoxide, J. Geophys. Res., 105, 24251–24261, 2000.

IPCC: Climate Change 2007: The Physical Science Basis, Contribution of Working Group I to the Fourth Assessment Report of the Intergovernmental Panel on Climate Change, edited by: Solomon, S., Qin, D., Manning, M., Chen, Z., Marquis, M., Averyt, K. B., Tignor, M., and Miller, H. L., 996 pp., Cambridge University Press, Cambridge, UK and New York, NY, USA, 2007.

Kaneyasu, N., Igarashi, Y., Sawa, Y., Takahashi, H., Takada, H., Kumata, H., and Höller, R.: Chemical and optical properties of 2003 Siberian forest fire smoke observed at the summit

ACPD

10, 15167–15196, 2010

of Mt. Fuji, Japan, J. Geophys. Res., 112, D13214, doi:10.1029/2007JD008544, 2007.
Jacob, D. J., Crawford, J. H., Maring, H., Clarke, A. D., Dibb, J. E., Ferrare, R. A., Hostetler, C. A., Russell, P. B., Singh, H. B., Thompson, A. M., Shaw, G. E., McCauley, E., Pederson, J. R., and Fisher, J. A.: The ARCTAS aircraft mission: design and execution, Atmos. Chem. Phys. Discuss., 9, 17073–17123, doi:10.5194/acpd-9-17073-2009, 2009.
Koch, D. and Hansen, J.: Distant origins of Arctic black carbon: A Goddard Institute for Space Studies ModelE experiment, J. Geophys. Res., 110, D04204, doi:10.1029/2004JD005296, 2005.
Koch, D., Schulz, M., Kinne, S., McNaughton, C., Spackman, J. R., Balkanski, Y., Bauer, S., Berntsen, T., Bond, T. C., Boucher, O., Chin, M., Clarke, A., De Luca, N., Dentener, F., Diehl, T., Dubovik, O., Easter, R., Fahey, D. W., Feichter, J., Fillmore, D., Freitag, S., Ghan, S., Ginoux, P., Gong, S., Horowitz, L., Iversen, T., Kirkevåg, A., Klimont, Z., Kondo, Y., Krol, M., Liu, X., Miller, R., Montanaro, V., Moteki, N., Myhre, G., Penner, J. E., Perlwitz, J., Pitari, G., Reddy, S., Sahu, L., Sakamoto, H., Schuster, G., Schwarz, J. P., Seland, Ø., Stier, P., Takegawa, N., Takemura, T., Textor, C., van Aardenne, J. A., and Zhao, Y.: Evaluation of black carbon estimations in global aerosol models, Atmos. Chem. Phys., 9, 9001–9026, doi:10.5194/acp-9-9001-2009, 2009.
Law, K. S. and Stohl, A.: Arctic air pollution: Origins and impacts, Science, 315, 1537–1540, 2007.
McConnell, J. R., Edwards, R., Kok, G. L., Flanner, M. G., Zender, C. S., Saltzman, E. S., Banta, J. R., Pasteris, D. R., Carter, M. M., Kahl, J. D. W., et al.: 20th-Century industrial black carbon emissions altered Arctic climate forcing, Science, 317, 1381–1384, 2007.
Neuman, J. A., Nowak, J. B., Huey, L. G., Burkholder, J. B., Dibb, J. E., Holloway, J. S., Liao, J., Peischl, J., Roberts, J. M., Ryerson, T. B., Scheuer, E., Stark, H., Stickel, R. E., Tanner, D. J., and Weinheimer, A.: Bromine measurements in ozone depleted air over the Arctic Ocean, Atmos. Chem. Phys. Discuss., 10, 3827–3860, doi:10.5194/acpd-10-3827-2010, 2010.
Quinn, P. K., Shaw, G., Andrews, E., Dutton, E. G., Ruoho-Airola, T., and Gong, S. L.: Arctic haze: current trends and knowledge gaps, Tellus B, 59, 99–114, 2007.
Ryerson, T. B., Buhr, M. P., Frost, G. J., Goldan, P. D., Holloway, J. S., Hubler, G., Jobson, B. T., Kuster, W. C., McKeen, S. A., Parrish, D. D., Roberts, J. M., Sueper, D. T., Trainer, M. T., Williams, J., and Fehsenfeld, F. C.: Emissions lifetimes and ozone formation in power plant plumes, J. Geophys. Res., 103, 22569–22583, 1998.
Schwarz, J. P., Gao, R. S., Fahey, D. W., Thomson, D. S., Watts, L. A., Wilson, J. C., Reeves, J.

ACPD
10, 15167–15196, 2010

M., Darbeheshti, M., Baumgardner, D. G., Kok, G. L., Chung, S. H., Schulz, M., Hendricks, J., Lauer, A., Karcher, B., Slowik, J. G., Rosenlof, K. H., Thompson, T. L., Langford, A. O., Loewenstein, M., and Aikin, K. C.: Single-particle measurements of midlatitude black carbon and light-scattering aerosols from the boundary layer to the lower stratosphere, J. Geophys. Res., 111, D16207, doi:10.1029/2006JD007076, 2006.

Schwarz, J. P., Spackman, J. R., Fahey, D. W., Gao, R. S., Lohmann, U., Stier, P., Watts, L. A., Thomson, D. S., Lack, D. A., Pfister, L., Mahoney, M. J., Baumgardner, D., Wilson, J. C., and Reeves, J. M.: Coatings and their enhancement of black carbon light absorption in the tropical atmosphere, J. Geophys. Res., 113, D03203, doi:10.1029/2007JD009042, 2008.

Sharma, S., Andrews, E., Barrie, L. A., Ogren, J. A., and Lavoué, D.: Variations and sources of the equivalent black carbon in the high Arctic revealed by long-term observations at Alert and Barrow: 1989–2003, J. Geophys. Res., 111, D14208, doi:10.1029/2005JD006581, 2006.

Shindell, D. T., Chin, M., Dentener, F., Doherty, R. M., Faluvegi, G., Fiore, A. M., Hess, P., Koch, D. M., MacKenzie, I. A., Sanderson, M. G., Schultz, M. G., Schulz, M., Stevenson, D. S., Teich, H., Textor, C., Wild, O., Bergmann, D. J., Bey, I., Bian, H., Cuvelier, C., Duncan, B. N., Folberth, G., Horowitz, L. W., Jonson, J., Kaminski, J. W., Marmer, E., Park, R., Pringle, K. J., Schroeder, S., Szopa, S., Takemura, T., Zeng, G., Keating, T. J., and Zuber, A.: A multi-model assessment of pollution transport to the Arctic, Atmos. Chem. Phys., 8, 5353–5372, doi:10.5194/acp-8-5353-2008, 2008.

Shindell, D. and Faluvegi, G.: Climate response to regional radiative forcing during the twentieth century, Nat. Geosci., 2, 294–300, doi:101038/NGEO473, 2009.

Simpson, W. R., von Glasow, R., Riedel, K., Anderson, P., Ariya, P., Bottenheim, J., Burrows, J., Carpenter, L. J., Frieß, U., Goodsite, M. E., Heard, D., Hutterli, M., Jacobi, H.-W., Kaleschke, L., Neff, B., Plane, J., Platt, U., Richter, A., Roscoe, H., Sander, R., Shepson, P., Sodeau, J., Steffen, A., Wagner, T., and Wolff, E.: Halogens and their role in polar boundary-layer ozone depletion, Atmos. Chem. Phys., 7, 4375–4418, doi:10.5194/acp-7-4375-2007, 2007.

Slowik, J. G., Cross, E. S., Han, J.-H., Davidovits, P., Onasch, T. B., Jayne, J. T., Williams, L. R., Canagaratna, M. R., Worsnop, D. R., Chakrabarty, R. K., Moosmuller, H., Arnott, W. P., Schwarz, J. P., Gao, R.-S., Fahey, D. W., Kok, G. L., and Petzold, A.: An inter-comparison of instruments measuring black carbon content of soot particles, Aerosol Sci. Tech., 41, 295–314, 2007.

Spackman, J. R., Schwarz, J. P., Gao, R. S., Watts, L. A., Thomson, D. S., Fahey, D. W., Holloway, J. S., de Gouw, J. A., Trainer, M., and Ryerson, T. B.: Empirical correlations between

ACPD
10, 15167–15196, 2010

black carbon aerosol and carbon monoxide in the lower and middle troposphere, Geophys. Res. Lett., 35, L19816, doi:10.1029/2008GL035237, 2008.
Stohl, A.: Characteristics of atmospheric transport in the Arctic troposphere, J. Geophys. Res., 111, D11306, doi:10.1029/2005JD006888, 2006.
Stone, R. S., et al.: A three-dimensional characterization of Arctic aerosols from airborne sun photometer observations; PAM-ARCMIP – April 2009, J. Geophys. Res., accepted, 2010.
Warneke, C., Bahreini, R., Brioude, J., Brock, C. A., de Gouw, J. A., Fahey, D. W., Froyd, K. D., Holloway, J. S., Middlebrook, A., Miller, L., Montzka, S., Murphy, D. M., Peischl, J., Ryerson, T. B., Schwarz, J. P., Spackman, J. R., and Veres, P.: Biomass burning in Siberia and Kazakhstan as an important source for haze over the Alaskan Arctic in April 2008, Geophys. Res. Lett., 36, L02813, doi:10.1029/2008GL036194, 2009.
Warneke, C., Froyd, K. D., Brioude, J., Bahreini, R., Brock, C. A., Cozic, J., de Gouw, J. A., Fahey, D. W., Ferrare, R., Holloway, J. S., Middlebrook, A. M., Miller, L., Montzka, S., Schwarz, J. P., Sodemann, H., Spackman, J. R., and Stohl, A.: An important contribution to springtime Arctic aerosol from biomass burning in Russia, Geophys. Res. Lett., 37, L01801, doi:10.1029/2009GL041816, 2010.

ACPD
10, 15167–15196, 2010

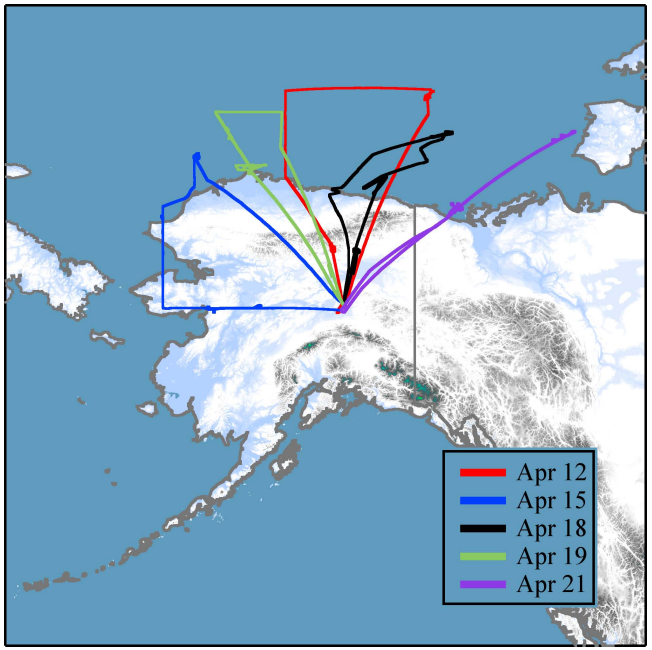

Fig. 1. The ARCPAC flight tracks for the data presented in this work (image courtesy of K. Aikin).

ACPD
10, 15167–15196, 2010

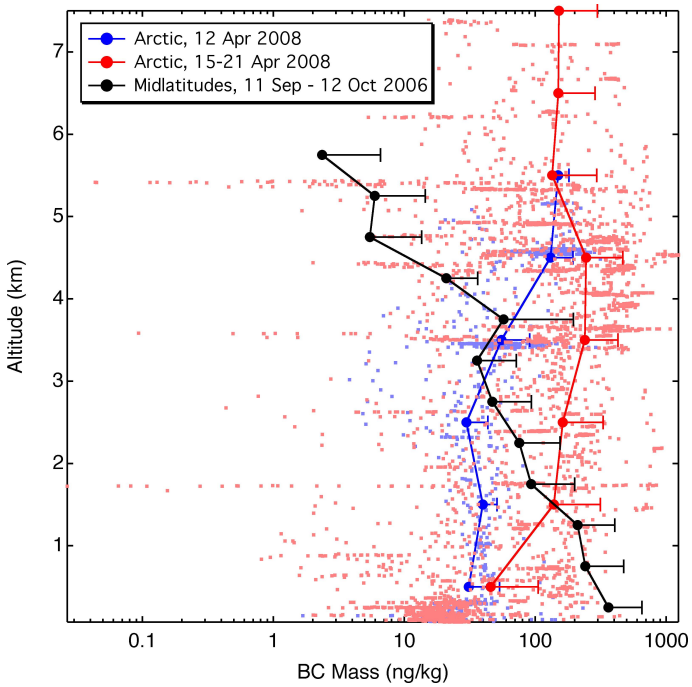

Fig. 2. Vertical profiles of BC mass mixing ratio for 5 flights in the Arctic during ARCPAC (blue and red data) and 16 flights at midlatitudes in eastern Texas during the Texas Air Quality Study (black curve). The data in blue are from 1 flight in the aged Arctic air mass, red from 4 flights in long-range biomass burning plumes. The small blue and red dots are 30-s averages of BC mass mixing ratio and the lines are 1-km mean values. The horizontal bars represent one standard deviation on both sides of the mean but are only drawn on the positive side for visual clarity.

ACPD
10, 15167–15196, 2010

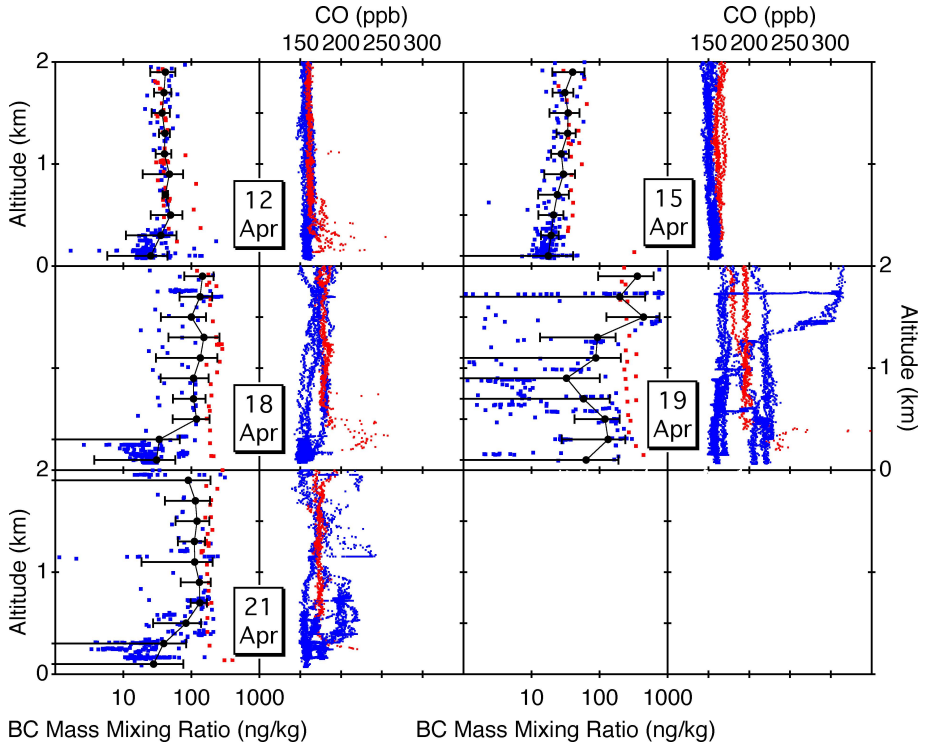

Fig. 3. Vertical profiles of BC mass and CO in the lowest 2-km altitude for all the flights during ARCPAC. The BC and CO data points are 30-s and 1-s data, respectively. The blue points denote BC data over the ice and open leads north of Alaska and the red points correspond to ascent/descent data at Fairbanks. The black line with bars represents mean BC mass with 1 standard deviation for 1-km altitude bins.

ACPD
10, 15167–15196, 2010




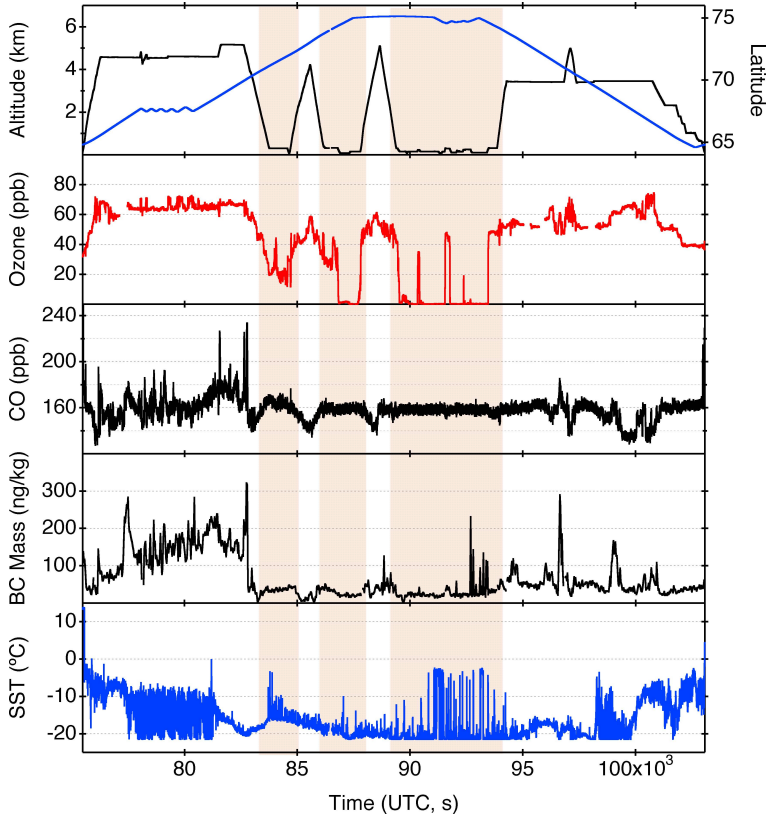

Fig. 4. Time series of altitude, latitude, ozone, CO, BC mass, and SST for the flight of 12 April 2008. The shaded segments highlight the parts of the flight where the NOAA WP-3D aircraft profiled the lowest 2-km altitude over the ice and open leads.

ACPD
10, 15167–15196, 2010

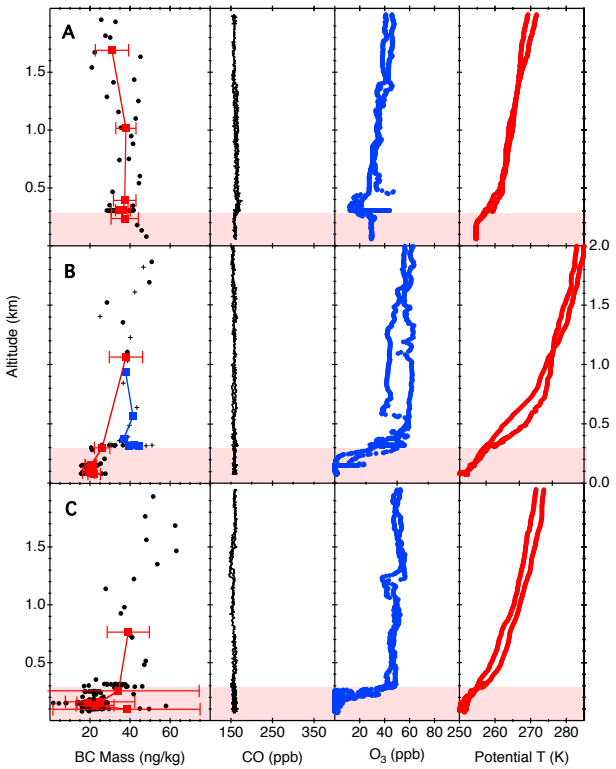

Fig. 5. Vertical profiles of BC mass, CO, ozone and potential temperature for the boundary layer flight segments on 12 April 2008 highlighted in Fig. 4. The gray-shaded regions represent the boundary layer. The profiles of BC mass (colored lines and markers) consist of mean values of BC mass binned by altitude where each bin represents an equal fraction of the data. The ascent (red line, circles) and descent data (blue line, plus markers) are segregated in **(b)**. The BC profiles consist of 30-s data and the CO, O_3, and potential temperature profiles are 1-s data.

ACPD
10, 15167–15196, 2010

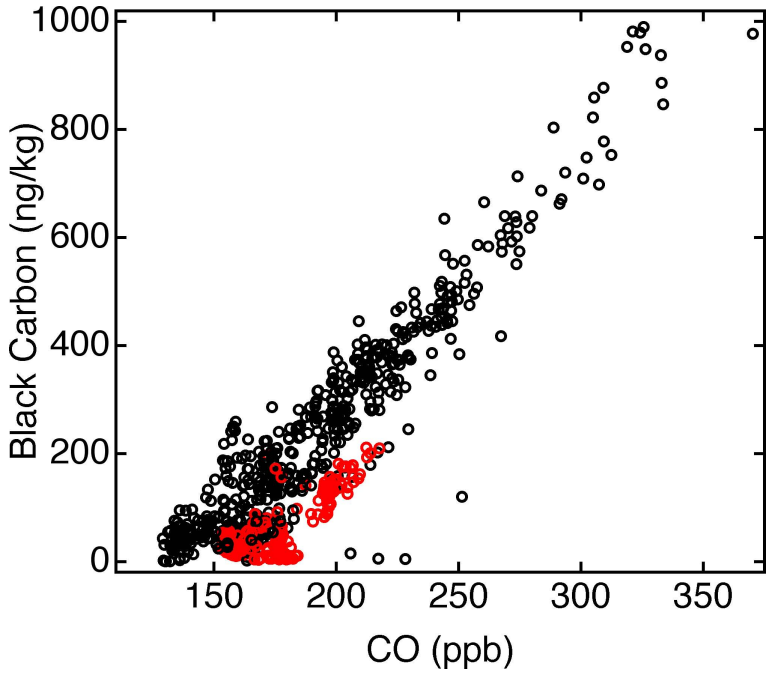

Fig. 6. Correlation between BC mass and CO for the 21 April flight. The 30-s data points are discriminated by altitude with the red points highlighting the correlation below 750 m and the black points denoting the rest of the data.

ACPD
10, 15167–15196, 2010

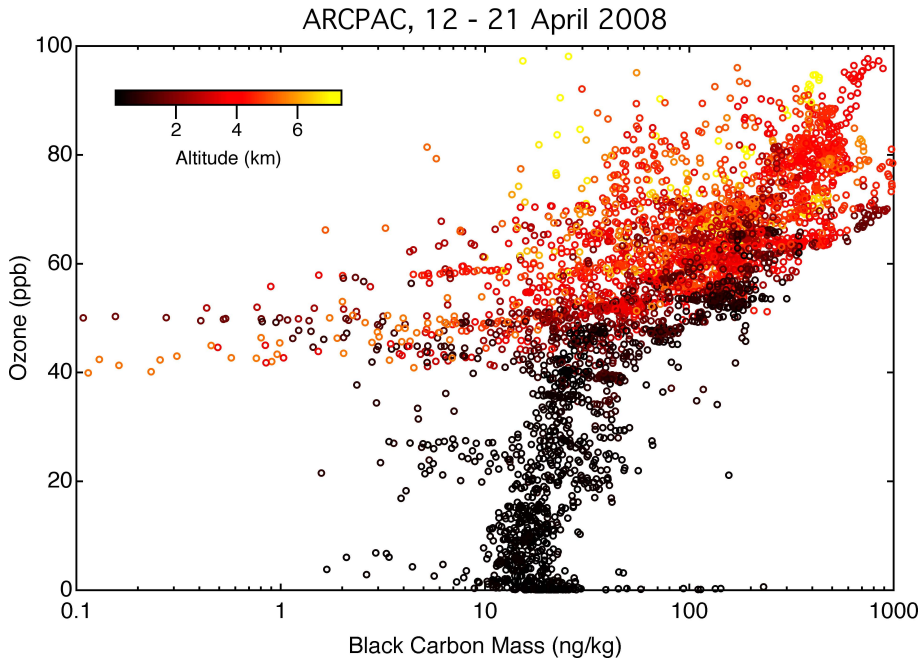

Fig. 7. Scatter plot of ozone and BC mass for 5 flights (12–21 April 2008) during ARCPAC. The data points are 30-s averages and color-coded by altitude.

ACPD
10, 15167–15196, 2010

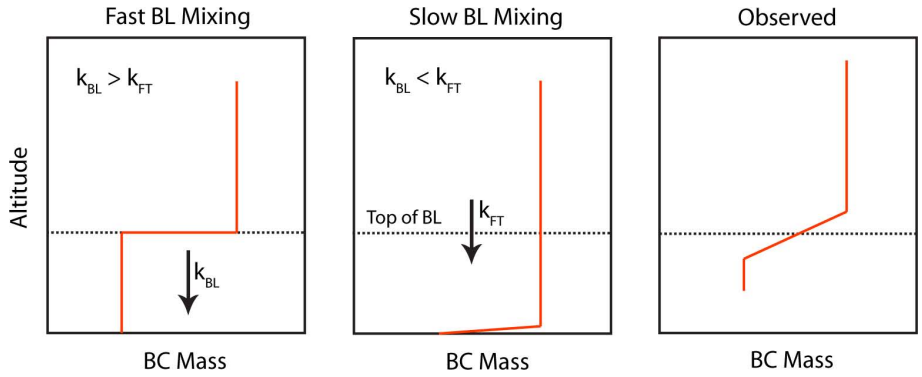

Fig. 8. Idealized and observed profiles in the springtime Arctic boundary layer. The first 2 profiles are idealized cases assuming BC is predominantly removed by dry deposition. The exchange coefficients k_{BL} and k_{FT} are the e-folding timescales for mixing in the boundary layer and mixing between the free troposphere and boundary layer, respectively. In the first case, the BL mixing is faster than mixing between the FT and BL. In the second case, BC is mixed from the FT into the BL as fast or faster than BL mixing. The third panel generalizes the observations presented here.

ACPD
10, 15167–15196, 2010

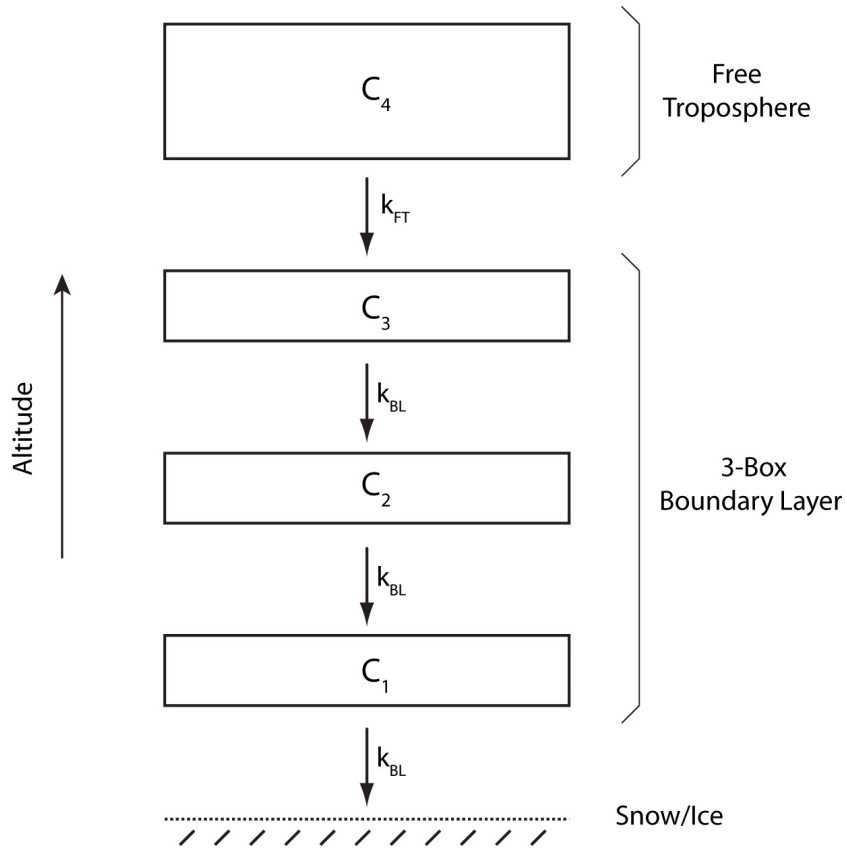

Fig. 9. Conceptual framework for a box model developed to examine the timescales for removal of BC from the Arctic boundary layer. The free troposphere and boundary layer are represented by the BC mass in box C_4 and boxes C_3–C_1, respectively. The exchange coefficients k_{FT} and k_{BL} are the same as defined in Fig. 8.

ACPD
10, 15167–15196, 2010

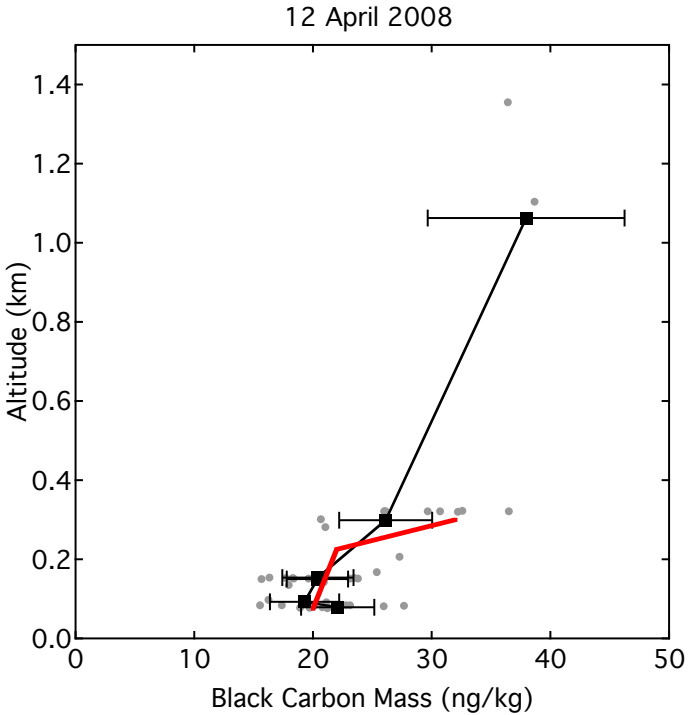

Fig. 10. Comparison between observed (black line) and simulated (red line) vertical profile of BC mass on 12 April 2008 as shown in Fig. 5b for the ascent profile. The error bars are 1 standard deviation around the observed mean in each equally weighted altitude bin. The gray points are the underlying 30-s BC data.

ACPD
10, 15167–15196, 2010